Spectral Radiative Properties of Fiberglass Insulation

H. Y. Yeh* and J. A. Roux†
University of Mississippi, University, Mississippi

An inversion method was used to determine the spectral radiative properties (scattering and absorption coefficients) of fiberglass insulation from directional-hemispherical reflectance data. The experimental reflectance data were obtained with a Willey 318S Fourier transform spectrophotometer (FTS) in the wavelength range of 4–19 μm. The theoretical reflectance values were computed from the discrete ordinates solution to the radiative transport equation. Both isotropic and anisotropic scattering were considered. The experimental data and theory were coupled via the nonlinear least squares method to invert the radiative properties. In the wavelength range of 20–80 μm, the extinction coefficient was inverted from specular reflectance data via Beer's law and the nonlinear least squares method. Heat fluxes were computed using these properties and compared to existing steady-state heat-transfer measurements.

Nomenclature

A_ℓ = ℓth coefficient of phase function Φ
a_ℓ = ℓth Gaussian quadrature weight
F_o = collimated flux
I = radiative intensity, W/m^2-steradian
I_o = collimated incident intensity
i = dimensionless intensity, $\pi I/Q''_o$
i_c = collimated component of i
i_d = diffuse component of i
i_o = dimensionless incident intensity
k = thermal conductivity, W/m-K
L = highest order of P_ℓ as used in Eq. (3)
M = number of Gaussian quadrature points
N = number of fiberglass samples
P_ℓ = Legendre polynominal of ℓth order
Q''_o = incident radiant heat flux
q''_o = dimensionless flux, Eq. (7)
R_d = directional-hemispherical reflectance
R_s = specular reflectance
y = spatial coordinate, cm
β = extinction coefficient, $\sigma + \kappa$, cm^{-1}
θ = polar angle
θ_d = polar angle of collimated incident intensity I_o
θ_s = polar angle of incident intensity for R_s
κ = absorption coefficient, cm^{-1}
λ = eigenvalue or wavelength, μm
μ = cosθ
μ_c = cosθ_d
μ_ℓ = ℓth Gaussian quadrature point
μ_s = cosθ_s
ρ_s = specular reflectivity of substrate
σ = scattering coefficient, cm^{-1}
τ = local optical thickness, βy
τ_o = total optical thickness
ϕ = azimuthal angle
Φ = phase function
Ω = solid angle
ω = albedo, $\sigma/(\sigma + \kappa)$
$\cap$ = hemisphere

Received Dec. 24, 1986; revision received April 9, 1987. Copyright © © American Institute of Aeronautics and Astronautics, Inc., 1987. All rights reserved.

*Presently with Energy and Mining Research Organization, Taiwan.
†Chairman, Mechanical Engineering. Member AIAA.

Introduction

THE coupled radiative and conductive heat-transfer problem in fiberglass attic insulation has been studied experimentally.[1–4] Although analytical techniques[5–12] are available for solving the coupled heat-transfer problem, results are still uncertain because of the lack of radiative properties (scattering and absorption coefficients). Since the key to computing heat transfer is reliable radiative properties, the present work focuses on determining the spectral radiative properties of low-density (10.9 kg/m^3) attic fiberglass insulation having a mean fiber diameter of about 9 μm. These radiative properties are needed to help thermal designers compute the transient and steady-state performance of a fiberglass attic insulation. These properties are also needed for optimization purposes and energy conservation.

Various approaches to determining radiative properties have been employed by several researchers.[13–17] The results in Fig. 1 show a significant variation among the extinction coefficients determined analytically and experimentally by various researchers. Figure 1 also shows the bulk fiberglass density of the insulation used by each researcher. Even combining the density and the extinction coefficient to obtain a mass extinction coefficient does not change the large spread in values, as shown in Fig. 1. A popular approach[13–15] is the use of Beer's law with normal transmittance data to determine the extinction coefficient. However, Beer's law does not account for the in-scattered intensity. Tong et al.[13] and Love and Saboonchi[14] only covered a small portion of the wavelength spectrum below 6.4 μm, which is not important for attic heat-transfer calculations. Although Chen[15] extended the properties out to 20 μm, the results are unclear because a slight density difference between his two sample sets yielded a large extinction coefficient difference. Chen measured the normal spectral transmittance with a Perkin-Elmer M621 spectrometer; Beer's law was used to determine the extinction coefficient in the 2.5–20 μm wavelength range.

Another method[16,17] employs the solution of Maxwell's equation for a single cylindrical fiber and considers the radiative properties to be a function of porosity, fiber diameter, fiber length, and fiber orientation. This method for determining radiative properties requires spectral optical properties (refractive index and absorption index) of fiberglass and the binder material. It was found that the extinction coefficients determined by this method were much higher than inferred by Beer's law. A more detailed literature review on the determination of radiative properties is given by Yeh.[18]

Generally, the experimental methods of the mentioned works[13–15] have several differences from the approach used in

the present work. First, the in-scattered intensity was not properly considered or was neglected.[13–15] The directional-hemispherical reflectance data and the analytical model used in this present work (4–19 μm) do account for the in-scattered radiation. When Beer's law is used, the in-scattered energy lowers the calculated β value. Secondly, to solve the radiative transport equation, an albedo was theoretically calculated,[17] and the two-flux model was used to solve the radiative heat-transfer problem. The present work employed the radiative transport equation to determine radiative properties and compute heat transfer. The Maxwell equation approach[16,17] seemed capable of handling the in-scattering intensity, the appropriate wavelength range, and the albedo problem mentioned, yet the analytically predicted properties as shown in Fig. 1 were generally much greater than the experimentally determined β values.[13–15]

The present method is different from the previously discussed works[13–17] and was used in the wavelength range of 4–19 μm. Albedo calculations were not made; rather, the albedo was determined from experimental data. Ideally, it is desirable to have spectral radiative properties out to 80 μm to cover most of the blackbody radiation at typical attic temperatures (273–350 K). However, present instrumentation capability restricted the directional-hemispherical reflectance measurements to $\lambda \leq 19$ μm.

The physical phenomenon was modeled with both isotropic and anisotropic scattering for one-dimensional radiative transport (see Fig. 2). The radiative transport equation was solved by the discrete ordinates method, which was developed by Chandrasekhar[5] and extended by Roux et al.[6] for computational usage. In the directional-hemispherical reflectance measurement, the radiative transport process was modeled as a collimated beam incident on a transparent interface at a polar angle of 15 deg. Multiple scattering and absorption inside the insulation were included.

The insulation samples were commercial pink fiberglass (density 10.9 kg/m^3) ranging in thickness from 0.112–1.28 cm. The substrate material was aluminum foil with a reflectivity of 0.97 in the infrared. The radiative properties were inverted by the nonlinear least squares method.[19] The values of the scattering and absorption coefficients, which minimized the sum of the squared error between the theoretical and the experimental reflectance values, were considered as the converged radiative properties.

In order to extend the nongray radiative heat-transfer calculations to 80 μm, specular reflectance data were measured with a Digilab FTS-20. Beer's law was used in the wavelength range of 20–80 μm with the nonlinear least squares method to determine the extinction coefficients. In the 20–80 μm region, the properties in this paper have the same difficulties as the other works[13–15] employing Beer's law. However, at typical attic temperatures, the 20–80 μm wavelength region contains less than 20% of the spectral blackbody radiant energy.

Experimental Measurements

Insulation samples were cut from a commercial pink fiberglass batt commonly used for residential attic application. In order to determine accurate radiative properties, the sample thicknesses were required to range from a very small thickness to a thickness that would simulate being semi-infinite (reflectance becomes independent of thickness). The samples were prepared to yield a significant change in reflectance with respect to sample thickness. The nine samples used in this work had the following distinct thicknesses (cm): 0.112, 0.168, 0.244, 0.320, 0.373, 0.513, 0.653, 0.866, and 1.28; the cross section of each sample was 3.18 cm × 3.18 cm. Details of the sample cutting and preparation are given in Ref. 18. Basically, the samples were prepared by slowly sinking a large block of fiberglass insulation in water. The block was then frozen solid. From the large frozen block, the thin samples were sliced with a special sinusoidal bandsaw blade. Next, the samples were dried. The thicknesses were both directly measured and computed from the fiberglass density and sample cross-sectional area. The directly measured and computed thicknesses had to agree before a sample was considered acceptable. The sample thicknesses have an uncertainty of about 5%; the radiative properties will be affected by about the same percentage. The radiative properties are influenced more by the accuracy of the radiometric measurements than by sample thickness uncertainties. An aluminum foil substrate ($\rho_s = 0.97$) was used under the samples while the reflectance measurements were made. The foil substrate was useful for maximizing the change in reflectance with respect to sample thickness.

The spectral directional-hemispherical reflectance measurement for each sample was made with the Willey 318S at an incidence angle of 15 deg (see Fig. 3). This instrument employed a roughened, gold-coated integrating sphere attached to a Fourier transform spectrometer, which uses an LN_2-cooled mercury cadmium teluride (HgCdTe) detector. This configuration allows measurements to be made in the 3–20 μm wavelength region. The fiberglass reflectance data are shown in Fig. 4. The curve labeled R_d is the directional-hemispherical reflectance data, and the curves labeled R_{s1} and R_{s2} are the specular reflectance data. Because of instrument noise at the two ends of the R_d spectra, data at wavelengths less than 4 μm and greater than 19 μm were not used. The acceptable signal to noise ratio (S/N) cutoff value of 100:1 was used. The noise was reduced by using 16 scans; with an FTS system, this amounted to an S/N improvement of a factor of $\sqrt{16}$ or 4.

A Digilab FTS-20 at the Oak Ridge National Laboratory was used to measure the specular reflectances R_s (R_{s1} and R_{s2}) at an incidence angle of 16 deg in the wavelength range of 3–80 μm. The sample specular reflectance data are also shown in Fig. 4 for the wavelength ranges of 3–25 μm (R_{s1}) and 20–80 μm (R_{s2}). Both R_{s1} and R_{s2} data were obtained with the same instrument (Digilab FTS-20) but with two different sets of optical components corresponding to the two different wavelength regions. A complete set of the data for all the samples is given in Ref. 18.

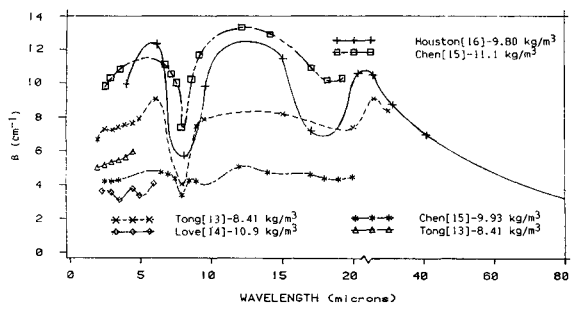

Fig. 1 Comparison of extinction coefficients from various researchers in the wavelength range of 2–80 μm.

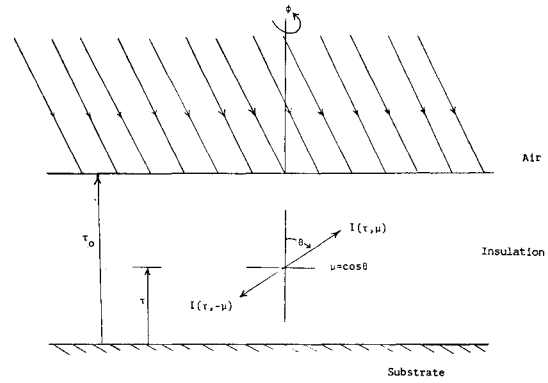

Fig. 2 Geometry and coordinate system for directional-hemispherical reflectance.

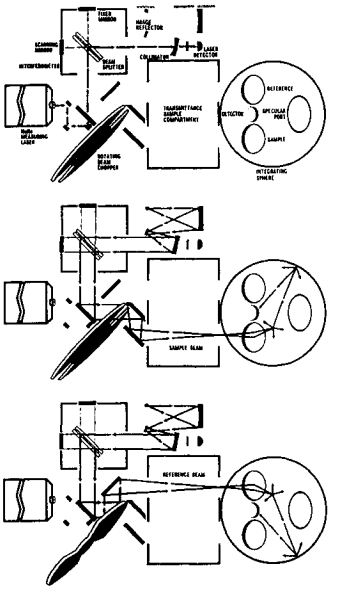

Fig. 3 Willey 318S Fourier transform infrared spectrophotometer reflectometer (with permission from Willey Corporation).

Analysis

The reflectance data obtained with the Willey 318S (Fig. 3) corresponds to the directional-hemispherical reflectance R_d (see Fig. 2), which is defined as the ratio of total reflected radiant flux to the incident collimated radiant flux Q_o'' and mathematically can be written as

$$R_d = \frac{1}{Q_o''} \int_{\Omega} I(\tau_0,\mu)\mu \, d\Omega \tag{1}$$

The intensity I was multiplied by π/Q_o'' to obtain a dimensionless intensity i. The intensity was obtained by solving the following nonemitting and azimuthally symmetric (angle of incidence near normal, 15 deg) scattering radiative transport equation:

$$\mu \frac{di(\tau,\mu)}{d\tau} = -i(\tau,\mu) + \frac{\omega}{4\pi} \int_0^{2\pi} \int_{-1}^{1} i(\tau,\mu')\Phi(\mu,\mu') \, d\mu' d\phi' \tag{2a}$$

with a specularly reflecting substrate

$$i(\tau,\mu)|_{\tau=0} = \rho_s \, i(\tau,-\mu)|_{\tau=0} \tag{2b}$$

and a transparent top boundary with a collimated incident intensity i_o

$$i(\tau,-\mu)|_{\tau=\tau_o} = i_o \tag{2c}$$

The azimuthally symmetric scattering phase function Φ in Eq. (2a) can be expressed in a Legendre polynominal series as

$$\Phi(\mu,\mu') = \sum_{\ell=0}^{L} A_\ell P_\ell(\mu) P_\ell(\mu') \tag{3}$$

The radiant intensity I_o of the incident collimated beam can be expressed in terms of Dirac delta functions as

$$I_o = F_o \delta(\mu - \mu_c)\delta(\phi - \phi_c) \tag{4}$$

where μ_c and ϕ_c define the incident direction and F_o is a constant. The incident collimated radiant heat flux Q_o'' is obtained by integrating I_o hemispherically and becomes

$$Q_o'' = F_o \, \mu_c \tag{5}$$

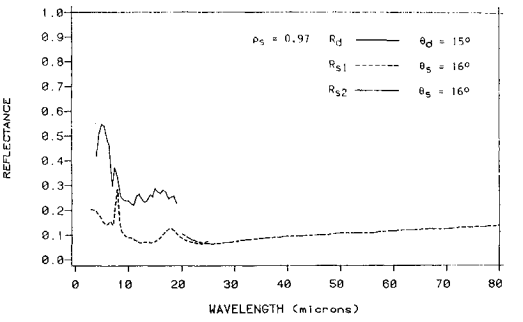

Fig. 4 Comparison of directional-hemispherical reflectance with specular reflectance for sample thickness 0.168 cm in the wavelength range of 3–80 μm.

Then I_o and Q_o'' can also be multiplied by π/Q_o'' to obtain dimensionless quantities i_o and q_o'' respectively as

$$i_o = \frac{\pi}{\mu_c} \delta(\mu - \mu_c)\delta(\phi - \phi_c) \tag{6}$$

and

$$q_o'' = \pi \tag{7}$$

The intensity i in Eq. (2) can be decomposed into two components, a collimated component i_c and a diffuse component i_d, with

$$i = i_c + i_d \tag{8}$$

Then Eqs. (2a–2c) can be decomposed[18,23,24] into two independent sets of equations, one set governing the behavior of i_c and the other set describing the behavior of i_d. The solution of i_c for $\mu > 0$ was obtained[18] as

$$i_c(\tau,-\mu) = i_o \, e^{-(\tau_o - \tau)/\mu}, \qquad \mu > 0 \tag{9}$$

The specular reflectance R_s can be calculated from Eq. (9), yielding

$$R_s = \rho_s e^{-2\tau_o/\mu_s} \tag{10}$$

where μ_s is the cosine of the incidence angle (16 deg) in the specular reflectance measurement.

The governing equation and boundary conditions for i_d are given in discrete ordinates form by Chandrasekhar[5] as

$$\mu_j \frac{di_d(\tau,\mu_j)}{d\tau} + i_d(\tau,\mu_j) = \frac{\omega}{2} \sum_{m=1}^{M} a_m i_d(\tau,\mu_m) \sum_{\ell=0}^{L} A_\ell P_\ell(\mu_j) P_\ell(\mu_m) + S_c(\tau,\mu_j), \qquad j = 1,2,\ldots M \tag{11a}$$

$$i_d(\tau,\mu_j)|_{\tau=0} = \rho_s i_d(\tau,-\mu_j)|_{\tau=0},$$

$$\mu_j > 0, \; j = 1,2,\ldots,M/2 \tag{11b}$$

$$i_d(\tau,-\mu_j)|_{\tau=\tau_o} = 0, \qquad j = 1,2,\ldots M/2 \tag{11c}$$

where

$$S_c(\tau,\mu_j) = \frac{\omega}{4\mu_c} e^{-(\tau_o - \tau)/\mu_c} \sum_{\ell=0}^{L} (-1)^\ell A_\ell P_\ell(\mu_j) P_\ell(\mu_c) + \frac{\omega}{4\mu_c} \rho_s e^{-(\tau_o + \tau)/\mu_c} \sum_{\ell=0}^{L} (-1)^\ell A_\ell P_\ell(\mu j) P_\ell(-\mu_c) \tag{11d}$$

and where the number of quadrature points M is an even number. The diffuse intensity i_d in Eq. (11a) can be split into a homogeneous solution i_h and a particular solution i_p:

$$i_d = i_h + i_p \tag{12}$$

The particular solution i_p is given[18] as

$$i_p(\tau,\mu_m) = \left[\frac{\omega}{4\mu_c} g_m(1/\mu_c)\right] e^{-(\tau_o-\tau)/\mu_c} + \left[\frac{\omega}{4\mu_c}\rho_s g_m(-1/\mu_c)\right] e^{-(\tau_o+\tau)/\mu_c} \tag{13}$$

where

$$g_m(1/\mu_c) = \sum_{\ell=0}^{L} \frac{A_\ell P_\ell(\mu_m)}{1+\mu_m/\mu_c}\gamma_0(1/\mu_c)\xi_\ell(1/\mu_c) \tag{14}$$

$$\xi_0 = 1,\ \xi_1(\lambda_j) = (\omega A_0 - 1)/\lambda_j \tag{15a}$$

$$\xi_{\ell+1}(\lambda_j) = \xi_\ell(\lambda_j)\frac{\omega A_\ell - (2\ell+1)}{\lambda_j(\ell+1)} - \frac{\ell\xi_{\ell-1}(\lambda_j)}{\ell+1},$$

$$\ell = 1,2,\ldots,L-1 \tag{15b}$$

$$\gamma_0(1/\mu_c) = \frac{1}{1-\sum_{k=0}^{L} A_k\xi_k(1/\mu_c)D_{0,k}(1/\mu_c)} \tag{16}$$

$$D_{\ell,k}(1/\mu_c) = \frac{\omega}{2}\sum_{j=1}^{M}\frac{a_j P_k(\mu_j)P_\ell(\mu_j)}{1+\mu_j/\mu_c}, \qquad \ell = 0 \tag{17}$$

The homogeneous solution i_h is given in Ref. 6. Finally, i_d can be obtained by summing up i_h and i_p as

$$i_d(\tau,\mu_m) = \sum_{j=1}^{M} C_j\frac{1-\lambda_j\mu_j}{1+\lambda_j\mu_m}e^{\lambda_j\tau}\sum_{\ell=0}^{L}A_\ell P_\ell(\mu_m)\xi_\ell(\lambda_j) + \frac{\omega}{4\mu_c}[g_m(1/\mu_c)e^{-(\tau_0-\tau)/\mu_c} + \rho_s g_m(-1/\mu_c)e^{-(\tau_0+\tau)/\mu_c}] \tag{18}$$

The eigenvalues λ_j shown in Eq. (18) can be determined from the characteristic equation

$$\frac{2}{\omega} = \sum_{m=1}^{M}\frac{a_m}{1+\lambda\mu_m}\sum_{\ell=0}^{L}A_\ell P_\ell(\mu_m)\xi_\ell(\lambda) \tag{19}$$

The integration constants C_j in Eq. (18) can be determined by inserting Eq. (18) into the boundary conditions, Eqs. (11b) and (11c). The directional-hemispherical reflectance R_d can then be expressed in terms of the dimensionless incident heat flux q''_o and intensity i as

$$R_d = \frac{1}{q''_o}\int_{\Omega}[i(\tau_o,\mu)]\mu\, d\Omega \tag{20a}$$

Inserting Eqs. (7) and (8) into Eq. (20a) yields

$$R_d = \frac{1}{\pi}\int_{\Theta}[i_c(\tau_o,\mu) + i_d(\tau_o,\mu)]\mu\, d\Omega \tag{20b}$$

The first term $i_c\mu$ was integrated analytically by replacing i_c from Eq. (9); the second term was integrated by Gaussian integration with the same quadrature order as used in Eq. (11a). Then, R_d can be written as

$$R_d = p_s e^{-2\tau_o/\mu_c} + 2\sum_{m=1}^{M/2} a_m i_d(\tau_o,\mu_m)\mu_m \tag{20c}$$

Finally, inserting Eq. (18) into Eq. (20c) yields

$$R_d = \rho_s e^{-2\tau_o/\mu_c} + 2\sum_{m=1}^{M/2} a_m\mu_m\left\{\sum_{j=1}^{M} C_j\frac{1-\lambda_j\mu_j}{1+\lambda_j\mu_m}e^{\lambda_j\tau_o} \times \sum_{\ell=0}^{L}A_\ell P_\ell(\mu_m)\xi_\ell(\lambda_j) + \frac{\omega}{4\mu_c}[g_m(1/\mu_c) + \rho_s g_m(-1/\mu_c)e^{-2\tau_o/\mu_c}]\right\} \tag{21}$$

The absorption and scattering coefficients were determined by the nonlinear least squares method.[19] The sum of the squares error between the experimental reflectance values of the N different samples R_j ($j = 1,\ldots,N$) and the theoretical directional-hemispherical reflectance [Eq. (21)] values R_{dj} ($j = 1,2,\ldots,N$) can be put into the form

$$E = \sum_{j=1}^{N}[R_j - R_{dj}]^2$$

where $R_{dj} = R_d(\sigma,\kappa,\mu_c,y_j)$ and y_j is the jth sample thickness. The minimum value of E corresponds to the converged values of σ and κ. A minimum E requires

$$\frac{\partial E}{\partial\sigma} = 0, \qquad \frac{\partial E}{\partial\kappa} = 0 \tag{22a,b}$$

Performing the differentiations in Eqs. (22a) and (22b) and then approximating R_{dj} by a first-order Taylor series expansion with respect to guessed values σ_o and κ_o, the result[18,19] becomes

$$\Delta\kappa\sum_{j=1}^{N}\left(\frac{\partial R_{dj}}{\partial\sigma}\right)\left(\frac{\partial R_{dj}}{\partial\kappa}\right) + \Delta\sigma\sum_{j=1}^{N}\left(\frac{\partial R_{dj}}{\partial\sigma}\right)^2 = \sum_{j=1}^{N}\left(\frac{\partial R_{dj}}{\partial\sigma}\right)(R_j - R_{dj}) \tag{23a}$$

$$\Delta\kappa\sum_{j=1}^{N}\left(\frac{\partial R_{dj}}{\partial\kappa}\right)^2 + \Delta\sigma\sum_{j=1}^{N}\left(\frac{\partial R_{dj}}{\partial\sigma}\right)\left(\frac{\partial R_{dj}}{\partial\kappa}\right) = \sum_{j=1}^{N}\left(\frac{\partial R_{dj}}{\partial\kappa}\right)(R_j - R_{dj}) \tag{23b}$$

where

$$\Delta\sigma = \sigma - \sigma_o \quad \text{and} \quad \Delta\kappa = \kappa - \kappa_o$$

The derivatives in Eqs. (23a) and (23b) were evaluated by finite differences. The values $\Delta\sigma$ and $\Delta\kappa$, which can be solved by employing Cramer's rule on Eqs. (23a) and (23b), were added to the previous iteration values of σ and κ to yield new improved values of σ and κ. These values are used again in Eqs. (23a) and (23b) to progressively yield more improved values of σ and κ. This iteration process is repeated until σ and κ values between two successive iterations were within one percent of one another. This procedure was performed at discrete wavelengths, every 0.5 μm from 4–19 μm. The number of iterations to obtain converged values of σ and κ was typically about four. Total calculation time for all 31 wavelengths was less than 1.2 min of CPU time on an AMDAHL V8 with an IBM 370 operating system.

Results and Discussion

The σ and κ values for pink residential fiberglass insulation were obtained by the method described. Two phase functions, isotropic scattering and anisotropic scattering, were used for inverting the radiative properties. The experimentally determined anisotropic forward scattering phase function for fiberglass insulation from Scheutz[21] at $\lambda = 9.65$ μm was employed in the 4–19 μm wavelength region. Using a laser, Scheutz[21] experimentally measured the phase functions for both fiberglass and foam insulations. These phase functions were then fit with Legendre polynomials and coefficients that could be directly used in this present work.

After converging on a pair of spectral σ and κ values, these properties were used in the computer model to compute R_d values. A comparison of the computed R_d values for isotropic

and anisotropic scattering and the actual experimental data are shown in Fig. 5 at a wavelength of 12.00 μm. The agreement shown in Fig. 5 is typical of the agreement between theory and data for all wavelengths. Although the radiative properties resulting from the two different phase function assumptions were quite different in magnitude, the agreement of the theoretical reflectance R_d and the experimental data were both very good. The heat-transfer results presented later will show good agreement between the use of isotropic and anisotropic radiative properties. In addition, the scaling of Lee and Buckius[21] will be shown to be valid.

The spectral absorption coefficient behavior was found to be essentially independent of phase function, as seen from Fig. 6. However, the spectral scattering coefficient, as shown in Fig. 7, was found to be highly phase function -dependent, as would be expected. The highly forward scattering phase function (anisotropic) as compared to the isotropic scattering has yielded higher scattering coefficient values (Fig. 7) and consequently has yielded higher spectral albedo values, as shown in Fig. 8 for the 4–19 μm wavelength region. As long as the phase function and scattering coefficient are used together and the scaling laws[21] are satisfied, the heat-transfer computations will be essentially the same (within about 2% or less).

In order to perform nongray heat-transfer calculations, it was necessary to obtain radiative properties in the 20–80 μm region. This region contains less than 20% of the total blackbody energy for typical attic temperatures. To obtain these properties, the specular reflectance data were employed. A pure attenuation process was assumed to be valid for the radiative transport within samples for which a specular reflectance measurement was made. Here, pure attenuation means that Beer's law considers scattering to be only an attenuation process, whereas the radiative transport equation describes scattering as both an attenuation process and an augmentation process. Thus, the only radiative property that could be inverted was the extinction coefficient. The spectral extinction coefficients were obtained by employing the nonlinear least squares procedure on the experimental data and Beer's law (Eq. 10). The Beer's law β values as shown in Fig. 9 compared more favorably with the anisotropic β value obtained from the transport equation than with the isotropic values. Therefore, the β values from Beer's law were used for nongray anisotropic radiative heat-transfer calculations from 20–80 μm. Since the heat transfer is not strongly dependent on ω between 0.1 and 0.7[12] and ω is not known in the 20–80 μm region, the constant values 0.398 and 0.155 (Fig. 8) were chosen to be the anisotropic and isotropic albedo values, respectively, for heat-transfer calculations. These two constant values were computed as the average albedo value in the 12–19 μm wavelength region. The constant value of albedo from 20–80 μm would imply that the slow increase in R_s in Fig. 4 with respect to wavelength is primarily due to β decreasing with wavelength; this is precisely the trend observed in Fig. 10. It is hoped that in the future, an instrument can be developed for measuring R_d out to 80 μm so both β and ω can be inverted directly in the 20–80 μm region.

It is appropriate to recommend a set of spectral radiative properties to be used for a heat-transfer calculation. Radiative properties to perform the heat-transfer calculations for the wavelength range of 4–80 μm are presented in Fig. 8 for ω and in Fig. 10 for β. For both isotropic and anisotropic scattering in the spectral range of 4–9 μm, the ω and β values shown in Figs. 8 and 10 were computed from Figs. 6 and 7. The anisotropic extinction coefficients in the spectral range of 20–80 μm were obtained from the Beer's law results shown in Fig. 9. The isotropic β values shown in Fig. 10 for the 20–80 μm region were obtained by using the $A_1/3$ scaling of Lee and Buckius[21] to scale from anisotropic to isotropic. These scaled β values are believed to be reliable because, as seen in Fig. 11, the β values scaled from anisotropic to isotropic in the 4–19 μm region agree very well with the directly computed isotropic β

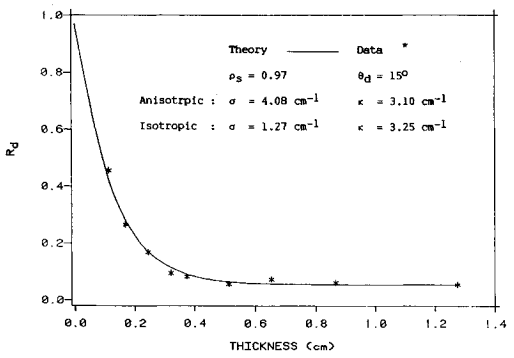

Fig. 5 Comparison of data and theoretical values for isotropic and anisotropic scattering using the inverted radiative properties at $\lambda = 12.00$ μm.

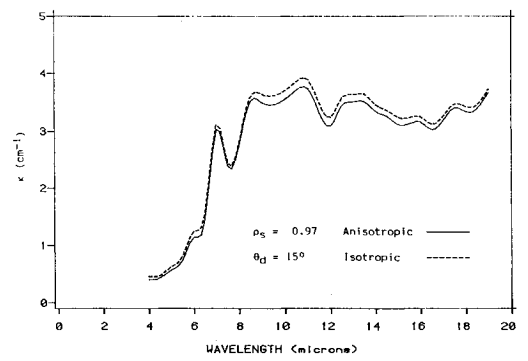

Fig. 6 Comparison of absorption coefficients for anisotropic and isotropic scattering.

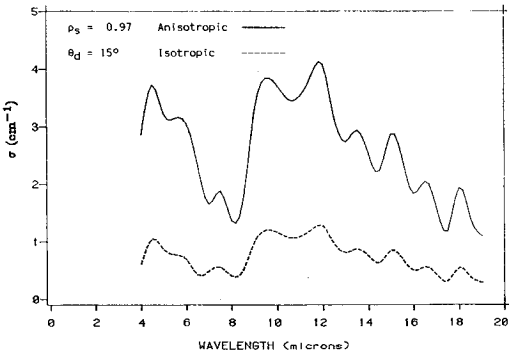

Fig. 7 Comparison of scattering coefficients for anisotropic and isotropic scattering.

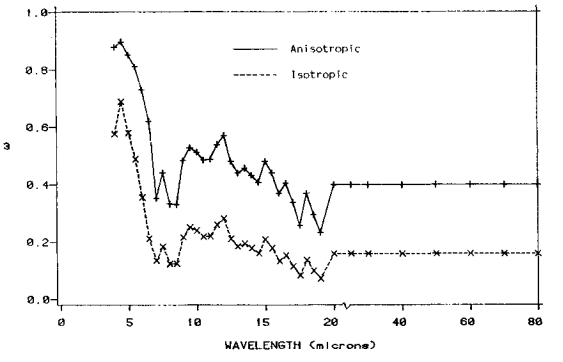

Fig. 8 Albedo values recommended for heat-transfer calculations.

values from the transport equation. Since the directly computed isotropic and scaled isotropic β values agree very well, it is implied that the heat-transfer results computed from both the isotropic and anisotropic properties should also be in good agreement. This will be demonstrated in Table 1.

The spectral extinction coefficients obtained in this work, shown in Fig. 10, are highly wavelength-dependent. The peaks in the extinction coefficient near 10 μm and 25 μm agree well with the peaks in Fig. 1 from the works of Houston and Korpela[16] and also with Tong and Tien.[17] The two peaks in the β curves in Fig. 10 near 10 μm and 25 μm correspond to the regions where most glasses typically have large values of absorption index (the imaginary part of the complex refractive index). The magnitude of the β values determined in this work were closer to the values obtained by Chen.[15] The average β values for Chen's low density (9.93 kg/m^3) were between the isotropic gray β value (3.70 cm^{-1}) and the anisotropic gray β value (5.47 cm^{-1}) of this work.

As shown in Table 1, the steady-state nongray and gray heat-transfer solutions were compared to the experimental data obtained by Houston and Korpela;[16] the experimental heat-transfer data[16] were taken as the standard for purposes of comparison. The nongray heat-transfer calculation[22] was performed by using a nine-band picket fence model with the properties shown in Fig. 8 for ω and Fig. 10 for β. The gray properties used here were the average values of the spectral properties (Figs. 6 and 7) in the wavelength range 4–19 μm. The hot-plate temperature T_s, the cold-plate temperature T_o, and the total heat fluxes were measured[16] by using a guarded hot-plate method (ASTM C-177). The emissivity of the two plates was 0.83, and the spacing between the plates, filled with fiberglass insulation, was 3.8 cm. The inverted nongray radiative properties (see Figs. 8 and 10) were shown to predict the total heat flux to within 2.5% for anisotropic scattering and 3.4% for isotropic scattering (see Table 1) for all four temperature ranges (case I: 285.2–308.8 K, case II: 285.3–337.3 K, case III: 285.6–365.2 K, case IV: 285.7–392.7 K). These heat-transfer results show that the radiative properties recommended here are capable of yielding good agreement with actual heat-transfer data over a wide temperature range for fiberglass insulation. The total heat flux results presented in Table 1 for nongray anisotropic and isotropic scattering were found to have slightly better agreement with the data than the theoretical heat flux predictions (nongray) of Houston and Korpela.[16] For cases I and II (285.2–337.3 K), which correspond to a residential attic application, the agreement of the gray predictions to the standard had a smaller absolute percent error than the nongray computations. However, the nongray computation percent errors are essentially constant for the four different temperature ranges because the nongray model is able to account for the blackbody radiation shift (Wein's displacement law). This indicates that the spectral properties β and ω are good for nongray heat-transfer calculations over a wider temperature range.

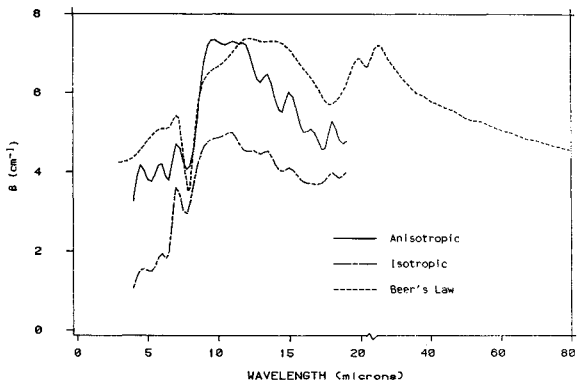

Fig. 9 Extinction coefficients for transport equation inversion and Beer's law inversion.

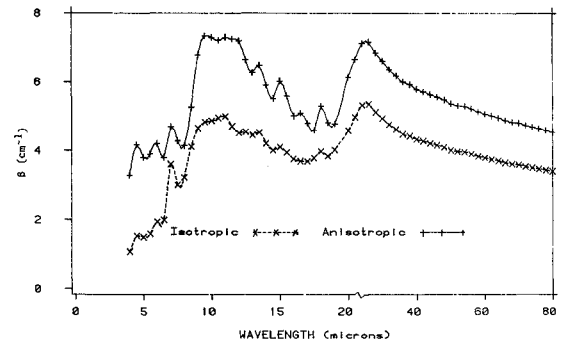

Fig. 10 Extinction coefficients recommended for heat-transfer calculations.

Table 1 Comparison of gray calculations with experimental data[16] and nongray calculations[16,22] for 3.8-cm-thick fiberglass insulation for steady-state heat transfer bounded by two plane surfaces[a] at temperatures T_s and T_o

	I	II	III	IV	Comments
			Boundary conditions		
T_s[b]	308.8	337.3	365.2	392.7	Ref. 16
T_o	285.2	285.3	285.6	285.7	Ref. 16
			Resultant heat flux		
q[c]	28.49	68.86	116.66	173.56	Data[16] (standard)
q	27.35	68.86	112.24	166.72	Ref. 16
e%[d]	−4.0	−3.7	−3.8	−3.9	
q	28.99	70.55	119.60	177.92	Nongray, nine bands[22]
e%	1.8	2.5	2.5	2.5	Anisotropic
q	29.27	71.19	120.67	179.49	Nongray, nine bands[22]
e%	2.8	3.4	3.4	3.4	Isotropic
q	28.46	68.09	113.32	165.18	Gray anisotropic
e%	−0.1	−1.1	−2.9	−4.8	$\beta = 5.47$ cm^{-1}, $\omega = 0.477$
q	28.83	69.03	114.97	167.70	Gray isotropic
e%	1.2	0.3	−51.5	−3.4	$\beta = 3.70$ cm^{-1}, $\omega = 0.201$

[a]Wall emissivities from Ref. 16 are 0.83. [b]Temperature, K. [c]q is total heat flux, W/m^2, including conduction and radiation. [d]e is percent error of q with respect to experimental data.[16] [e]Properties obtained from Figs. 8 and 10.

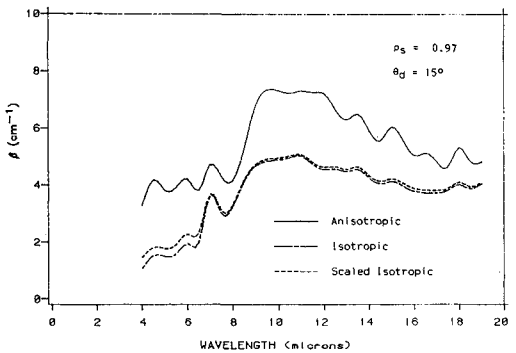

Fig. 11 Comparison of extinction coefficients for isotropic scattering and scaling from anisotropic scattering.

Conclusions

The spectral radiative properties σ and κ determined in this work were shown to be valuable for computing heat transfer. The assumption of phase function did not significantly influence the heat-transfer results as long as the same phase function was used for both property determination and heat-transfer computation. The method developed in this work is valuable for determining σ and κ values for multiple scattering media such as fiberglass, rockwool, and foam. A further improvement in the properties could be achieved by extending the measurement of R_d out to 80 μm; it is hoped to accomplish this measurement in the future.

Acknowledgment

This work was funded by the National Science Foundation under Grant MEA-8217974.

References

[1]Verschoor, J. D., Greebler, P., and Manville, N. J., "Heat Transfer by Gas Conduction and Radiation in Fibrous Insulations," *Transactions of ASME*, Vol. 74, 1952, pp. 961–968.

[2]Strong, H. M. Bundy, F. P., and Bovenkerk, H. P., "Flat Panel Vacuum Thermal Insulation," *Journal of Applied Physics*, Vol. 31, No. 1, 1960, pp. 39–50.

[3]Nathaniel, E. H. and Robin, C. S., "Radiant Heat Transfer in Fibrous Insulation," *Journal of Applied Physics*, Vol. 38, No. 12, 1967, pp. 4663–4668.

[4]Bankvall, C., "Heat Transfer in Fibrous Materials," *Journal of Testing and Evaluation*, Vol. 1, No. 3, May 1973, pp. 235–243.

[5]Chandrasekhar, S., *Radiative Transfer*, Dover, New York, 1960.

[6]Roux, J.A., Smith, A.M., and Todd, D. C., "Radiative Transfer with Anisotropic Scattering and Arbitrary Temperature for Plane Geometry," *AIAA Journal*, Vol. 13, Sept. 1975, pp. 1203–1211.

[7]Hottel, H. C. and Sarofim, A. F., *Radiative Transfer*, McGraw-Hill, New York, 1967.

[8]Ozisik, M. N., *Radiative Transfer*, Wiley, New York, 1973.

[9]Dayan, A. and Tien, C. L., "Heat Transfer in a Gray Planar Medium with Linear Anisotropic Scattering," *Journal of Heat Transfer*, Vol. 97, 1975, pp. 391–396.

[10]Yuen, W. W. and Wong, L. W., "Heat Transfer by Conduction and Radiation in a One-Dimensional Absorbing, Emitting and Anisotropically Scattering Medium," *Journal of Heat Transfer*, Vol. 102, 1980, pp. 303–307.

[11]Hsia, H. M. and Love, T. J., "Radiant Heat Transfer Between Parallel Plates Separated by a Non-Isothermal Medium with Anisotropic Scattering," *Journal of Heat Transfer*, Vol. 89, Aug. 1967, pp. 197–203.

[12]Roux, J. A., Yeh, H. Y., Smith, A. M., and Wang, S. Y., "Finite Element Analysis of Radiative Transport in Fibrous Insulation," *Journal of Energy*, Vol. 7, No. 6, Nov./Dec. 1983, pp. 702–709.

[13]Tong, T. W., Yang, Q. S., and Tien, C. L., "Radiative Heat Transfer in Fibrous Insulation—Part II: Experimental Study," *Journal of Heat Transfer*, Vol. 105, No. 1, 1983, pp. 76–81.

[14]Love, T. J. and Saboonchi, A., "Determination of the Extinction Coefficient of Glass Fiber Insulation," *AIAA 15th Thermophysics Conference*, AIAA-80-1528, 1980.

[15]Chen, F. F., *Energy Transfer in Fibrous Insulating Materials*, MS Thesis, University of Kentucky, Lexington, KY, 1979.

[16]Houston, R. L. and Korpela, S. A., "Heat Transfer through Fiberglass Insulation," *Proceedings of the 7th International Heat Transfer Conference*, Vol. 2, 1982, pp. 499–504.

[17]Tong, T. W. and Tien, C. L., "Radiative Heat Transfer in Fibrous Insulation—Part I: Analytical Study," *Journal of Heat Transfer*, Vol. 105, No. 1, 1983, pp. 70–75.

[18]Yeh, H. Y., *Radiative Properties and Heat Transfer Analysis of Fibrous Insulation*, Ph.D. Dissertation, The University of Mississippi, University, MS, 1986.

[19]Roux, J. A. and Smith, A. M., "Determination of Radiative Properties from Transport Theory and Experimental Data," AIAA Progress Series in Astronautics and Aeronautics: *Spacecraft Radiative Transfer and Temperature Control*, edited by T. E. Horton, Vol. 83, AIAA, New York, 1981, pp. 22–37.

[20]Scheutz, M. A., *Heat Transfer in Foam Insulations*, MS Thesis, MIT, Cambridge, MA, 1982.

[21]Lee, H. and Buckius, R. O., "Scaling Anisotropic Scattering in Radiation Heat Transfer for a Planer Medium," *Journal of Heat Transfer*, Vol. 104, Feb. 1982, pp. 68–75.

[22]Rish J. W. III and Roux, J. A., "Heat Transfer Analysis of Fibrous Insulations With and Without Radiant Barriers for Summer Conditions," *Journal of Thermophysics and Heat Transfer*, Vol. 1, Jan. 1987, pp. 43–49.

[23]Roux, J. A. and Smith, A. M., "Biangular Reflectance for an Absorbing and Isotropically Scattering Medium," *AIAA Journal*, Vol. 23, April 1985.

[24]Ozisik, M. W., *Radiative Transfer*, Wiley, New York, 1973.